High-order-harmonic generation in molecular sequential double ionization by intense circularly polarized laser pulses

Kai-Jun Yuan,* Huizhong Lu, and André D. Bandrauk†
Laboratoire de Chimie Théorique, Faculté des Sciences, Université de Sherbrooke, Sherbrooke, Québec, Canada J1K 2R1
(Received 12 April 2015; published 13 August 2015)

We present effects of electron energy transfer by electron collisions on high-order-harmonic generation (HHG) in molecular sequential double ionization by intense *circularly* polarized laser pulses. Results from numerical solutions of time-dependent Schrödinger equations for extended (large internuclear distance) H_2 where electrons are entangled and hence delocalized by exchange show that HHG with cutoff energy up to $I_p + 24U_p$ can be obtained, where I_p is the molecule ionization potential and $U_p = I_0/4\omega_0^2$ (in atomic units) is the ponderomotive energy for pulse intensity I_0 and frequency ω_0. A time-frequency analysis is employed to identify electron collisions for the generation of harmonics. Extended HHG arises from electron energy exchange, which agrees well with the prediction of a classical two electron collision model. Results for nonsymmetric HHe^+ where initially electrons are localized on He are also compared and confirm the role of initial electron delocalization via entanglement for obtaining extended HHG plateaus.

DOI: 10.1103/PhysRevA.92.023415 PACS number(s): 33.80.Rv, 42.65.Ky

I. INTRODUCTION

High-order-harmonic generation (HHG) in atoms and molecules as a source for producing attosecond (1 as = 10^{-18} s) pulses is of growing interest due to its possible use for monitoring electron dynamics [1–3]. To date the shortest *linearly* polarized single pulse with a duration of 67 as has been produced from HHG obtained with a linearly polarized few cycle intense infrared laser field in atoms [4]. One of the fundamental concepts of HHG has been the rescattering model in the presence of intense laser pulses [5]. Thus, following tunneling ionization, the electron remains "controlled" by the laser field, returning to the parent ion after a phase (sign) change of the electric field. This simple classical model of laser induced recollision with the parent ion has led to the development of a consistent theory of HHG in atoms [6] and molecules [7]. Two-color linearly polarized excitation schemes which have furthermore shown control of the recolliding electron, including preionization with nonzero initial velocity [8] instead of the zero initial velocity of the tunneling model [5], can be used to explore new possibilities for control of the HHG process. For nonlinear polarization, a zero-velocity electron can never return to the parent ion and only for the case of a nonzero initial velocity recollision is possible [9]. Recently many schemes, such as two coplanar counter-rotating circularly polarized fields [10,11] or combinations of circular polarization light and static or terahertz fields [12], have been proposed to efficiently produce *circularly* polarized HHG.

Collision with neighboring ions in stretched, large internuclear distance molecules leads to extended harmonic orders or energies in HHG [13–20], beyond the linearly polarized light recollision maximum energy law $N_m\hbar\omega_0 = I_p + 3.17U_p$, where I_p is the ionization energy and $U_p = I_0/4\omega_0^2$ (atomic units, a.u., are used unless otherwise noted) is the ponderomotive energy for a pulse maximum amplitude E_0, corresponding to intensity $I_0 = \frac{1}{2}c\varepsilon_0 E_0^2$ and angular frequency ω_0 [2,5–8]. In linearly polarized laser induced collisions with neighboring ions, maximum harmonic energies are given from the initial zero velocity ionization model by $I_p + 8U_p$ [13–20]. Collision with the parent or a neighboring ion leads to refocusing of the continuum electron wave packet [15], thus enhancing the efficiency [21]. It has been shown that in a one-color ultrashort intense laser pulse the maximum harmonic energy up to $I_p + 32U_p$ can be generated due to a second collision of the continuum electron with neighboring ions in both linear [16] and circular [20] polarizations. Of note is that for these extended harmonics the intensity drops dramatically as the energy increases, approximately ten orders, thus leading to very low efficiency for attosecond pulse generation.

Previous models have dealt with single electron collision for interpreting HHG processes [5,16]. Double ionization by circularly and elliptically polarized laser pulses in atomic and molecular systems has been attracting considerable attention in the past years, e.g., [22–25]. Recently it has been reported that recollision with circularly polarized light can be possible under certain conditions, resulting in HHG spectra by breaking normal selection rules [23]. In this paper we focus on sequential double ionization of two electron molecules in the presence of circularly polarized laser pulses. We theoretically investigate HHG spectra from numerical solutions of time-dependent Schrödinger equations (TDSEs). We report for H_2 the induced harmonics with cutoff up to $I_p + 24U_p$ obtained, beyond the predictions of the classical model for single electron neighbor collision with maximum energy $I_p + 8U_p$. We consider a classical two electron collision model and attribute the extended harmonics to electron energy exchange by collision in sequential double ionization. The mechanism of HHG is further characterized with a time frequency analysis.

II. NUMERICAL METHODS

Considering a static nuclear molecular system, the corresponding TDSE is written with respect to the center of mass

*kaijun.yuan@usherbrooke.ca
†andre.bandrauk@usherbrooke.ca

of two nuclei as

$$i\frac{\partial}{\partial t}\psi(1,2) = H(\mathbf{r},t)\psi(1,2) = \left(-\frac{1}{2}\nabla_{1,2}^2 + V_{ee} + V_{en} + V_L\right)\psi(1,2), \quad (1)$$

where $\nabla_{1,2}^2$ is the Laplacian, V_{ee} is the electron-electron repulsion, and the electron-proton attraction Coulomb potential is V_{en}, The reduced four-dimensional TDSE is described in polar coordinates $\mathbf{r} = (\rho,\theta)$ and numerically solved by a second-order split-operator method combined with a five-order finite-difference method and Fourier transform (FT) technique [26]. More details can be found in [27]. The laser-electron radiative coupling is described by the time-dependent potential V_L in the length gauge:

$$V_L = -E_0 f(t)\sum_{j=1}^{2}[\rho_j \cos\theta_j \cos(\omega_0 t) + \rho_j \sin\theta_j \sin(\omega_0 t)]. \quad (2)$$

$f(t)$ is the pulse envelope and E_0 is the field maximum amplitude for intensity $I_0 = c\varepsilon_0 E_0^2/2$. The HHG power spectrum $P_{x/y}(\omega)$ is obtained from the absolute square of the FT of the time-dependent dipole accelerations [28] $\langle\ddot{x}(t)\rangle$ and $\langle\ddot{y}(t)\rangle$:

$$P_\varsigma(\omega) = \left|\int \exp(-i\omega t)\langle\ddot{\varsigma}(t)\rangle dt\right|^2, \quad (3)$$

with the laser induced electron acceleration obtained from the time-dependent wave function $\psi(\mathbf{r},t)$:

$$\langle\ddot{\varsigma}(t)\rangle = \langle\psi(t)|-\partial H/\partial\varsigma|\psi(t)\rangle, \quad (4)$$

where $\varsigma = x,y$.

Extended molecules H_2 and HHe^+ are used at large internuclear distance $R = 22$ a.u. Such molecules have recently been produced by pump-probe techniques [29]. At large R the initial electronic state of H_2 involves a delocalized valence bond (Heitler-London) atomic configuration H $\cdots$ H:

$$\psi(1,2) = [1s_a(1)1s_b(2) + 1s_a(2)1s_b(1)]/\sqrt{2}, \quad (5)$$

where $1s_a$ and $1s_b$ denote the $1s$-like atomic orbitals on protons a and b, respectively, and 1 and 2 are the coordinates of the two electrons. For HHe^+ the initial electronic state reads as [30,31]

$$\psi(1,2) = 1s_b(2)1s_b(1), \quad (6)$$

where electrons are mainly localized on He. The exact initial wave function is calculated by propagating in imaginary time the zero-field molecular Hamiltonian in TDSEs in Eq. (1). The corresponding molecular ionization potentials are, respectively, $I_p = 0.5$ and 0.89 a.u. for H_2 and HHe^+ [31]. A ten cycle trapezoid circularly polarized laser pulse is used with intensity $I_0 = 2\times10^{14}$ W/cm^2 ($E_0 = 0.0755$ a.u.), wavelength $\lambda = 400$ nm ($\omega_0 = 0.114$ a.u., $\tau = 1.33$ fs), and duration $T = 10\tau = 13.3$ fs, where one cycle $\tau = 2\pi/\omega_0$. The ellipticity dependence of 400-nm-driven HHG has shown that high-harmonic yields decrease less as compared to 800-nm HHG, thus concluding that HHG signals are less susceptible to ellipticity at 400 nm [32]. We therefore focus on circularly polarized pulses at $\lambda = 400$ nm. The large time duration ensures the pulse area $\int E(t)dt = 0$ to eliminate static field effects in accordance with Maxwell's equations [2].

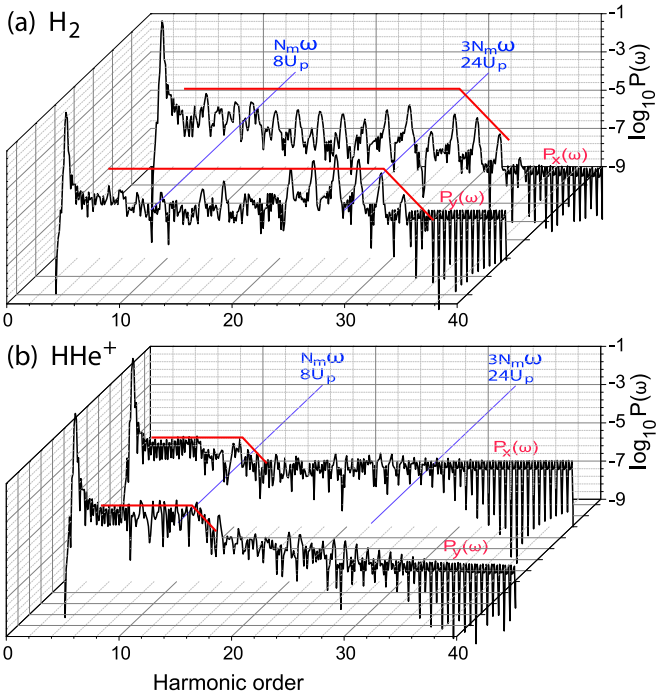

FIG. 1. (Color online) The x and y components of HHG spectra in x aligned two electron molecules (a) H_2 and (b) HHe^+ at internuclear distance $R = x(t_c) = 22$ a.u. with $\lambda = 400$ nm ($\omega = 0.114$ a.u., $\tau = 1.33$ fs), $I_0 = 2.0\times10^{14}$ W/cm^2 ($E_0 = 0.0755$ a.u.) circularly polarized light. The maximum harmonic energy predicted from the single electron collision model in Eq. (9) is $I_p + 8U_p$.

III. RESULTS AND DISCUSSIONS

Figure 1 shows results of HHG spectra of x aligned two electron systems, symmetric H_2, and nonsymmetric HHe^+ by solving corresponding TDSEs in Eq. (1). We see that for both H_2 and HHe^+ molecules at large internuclear distance $R = 22$ a.u. HHG spectra are efficiently produced in circularly polarized laser pulses due to electron collision with neighboring ions. A plateau is obtained with a cutoff in both x and y directions, as illustrated in Fig. 1. We emphasize that for equilibrium H_2 and HHe^+ molecules no harmonics can be appreciably produced due to the ionized electron's large radius inhibiting recollision with the parent ion [12,33]. We note, however, that the harmonic cutoff energies are different for symmetric H_2 and nonsymmetric HHe^+. In Fig. 1(a) for H_2, HHG spectra exhibit an intense large cutoff order, up to $N_c = 28$ corresponding to the energy $I_p + 24U_p$, whereas for HHe^+ in Fig. 1(b) a low order $N_c = 15$ around the harmonic energy $I_p + 8U_p$ is obtained and a second cutoff at $24U_p$ is very weak. Since the same ionizing pulses are used, the difference of the harmonic cutoff frequency indicates the influence of the electron structure of the molecular medium.

We turn to a classical model of electron collision with neighboring ions [12] for interpreting the results in Fig. 1. For a single frequency circularly polarized laser pulse $E_x(t) = E_0\cos\omega_0 t, E_y(t) = E_0\sin\omega_0 t$, the laser induced velocities

are

$$\dot{x}(t) = -\frac{E_0}{\omega_0}(\sin\omega_0 t - \sin\omega_0 t_0),$$
$$\dot{y}(t) = -\frac{E_0}{\omega_0}(\cos\omega_0 t_0 - \cos\omega_0 t), \tag{7}$$

for initial zero velocities $\dot{x}(t_0) = \dot{y}(t_0) = 0$ at initial time t_0. The average velocities $\langle\dot{x}(t)\rangle = E_0/\omega_0 \sin\omega_0 t_0$ and $\langle\dot{y}(t)\rangle = -E_0/\omega_0 \cos\omega_0 t_0$ are nonzero and are called *drift* velocities. Setting $t_0 = 0$ shows that a nonzero initial drift velocity always occurs perpendicular to the tunneling x direction [5]. The corresponding laser induced displacements are

$$x(t) = -\frac{E_0}{\omega_0^2}[\cos\omega_0 t_0 - \cos\omega_0 t - (\omega_0 t - \omega_0 t_0)\sin\omega_0 t_0],$$
$$y(t) = -\frac{E_0}{\omega_0^2}[\sin\omega_0 t_0 - \sin\omega_0 t + (\omega_0 t - \omega_0 t_0)\cos\omega_0 t_0]. \tag{8}$$

The time-dependent kinetic energies obtained from Eq. (7) are

$$K_e(t) = \frac{1}{2}[\dot{x}^2(t) + \dot{y}^2(t)]$$
$$= \left(\frac{E_0}{\omega_0}\right)^2 [1 - \cos(\omega_0 t - \omega_0 t_0)], \tag{9}$$

with maximum value $8U_p$ at $\omega_0 t_c - \omega_0 t_0 = (2n'+1)\pi$, $n' = 0,1,2,\ldots$, where t_c is the collision time of ionized electrons with neighboring ions. It should be noted that the maximum kinetic $8U_p$ energy cannot occur for linearly polarized laser pulses as the electron is ionized via tunneling since the electric field at the initial phase is zero since $\omega_0 t_0 = \pi/2$ and the tunneling probability is zero as well. The total displacements are a function of t_c:

$$R_{n'}(t_c) = [x^2(t_c) + y^2(t_c)]^{\frac{1}{2}}$$
$$= \frac{2E_0}{\omega_0^2}\left[1 + \left(n' + \frac{1}{2}\right)^2 \pi^2\right]^{\frac{1}{2}}. \tag{10}$$

For collisions of electrons with neighboring ions at time t_c to produce efficient maximum energy $8U_p$ in Eq. (9), the internuclear configuration and distance Eq. (10) is $R = R_c = R_0(t_c) = 22$ a.u., for $n' = 0$, the internuclear distance in Fig. 1.

One sees that the results in Fig. 1(b) of nonsymmetric HHe^+ where the two electrons are localized on He agree well with the theoretical predictions in Eqs. (7)–(10) with maximum harmonic energies $I_p + 8U_p$, similar as single electron H_2^+ systems [12]. However, for the symmetric H_2 molecular system where the electrons are *entangled* by Fermion antisymmetry requirements on the two different protons, the cutoff energy of the HHG spectra exceeds the predictions from Eq. (9), up to $I_p + 24U_p$ in Fig. 1(a). We show next that the extension of HHG for H_2 mainly results from the energy exchange of entangled electrons by collisions. In Figs. 2(a) and 2(b) we, respectively, illustrate evolutions of single electron wave-packet densities $|\psi(t)|^2$ of H_2 and HHe^+ at different times. The motions of electrons follow the laser fields with a counterclockwise direction. For HHe^+ the initial electron density is asymmetric with distribution of electrons mainly localized on He. As shown in Fig. 2(b), only one electron trajectory appears at each cycle. Driven

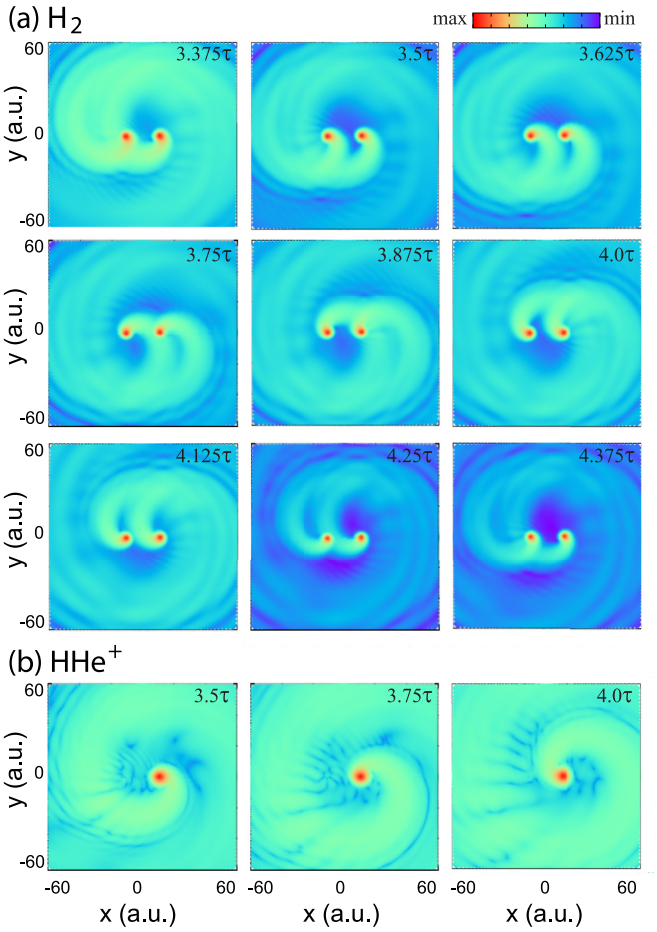

FIG. 2. (Color online) Evolutions of electron wave-packet densities $|\psi(x,y,t)|^2$ with time for (a) H_2 and (b) HHe^+ at $R = 22$ a.u. with intensity $I_0 = 2\times10^{14}$ W/cm^2 and wavelength $\lambda = 400$ nm ($\tau = 1.33$ fs) circularly polarized laser pulses, corresponding to Figs. 1(a) and 1(b).

by the circularly polarized light the electron wave packets move from the right atom He to the left H where there are no electrons initially, which leads to HHG spectra with maximum energy $I_p + 8U_p$, according to the classical collision model in Eqs. (7)–(10). However, for the delocalized entangled valence atomic configuration $H\cdots H$, the same ionization amplitudes from the two centers lead to two electron collision trajectories at each cycle in Fig. 2(a), which offer the possibility to exchange kinetic energies by a collision with each other. We show in Fig. 3 the time frequency analysis of harmonics for both H_2 and HHe^+, which provides the collision time of the ionized electron with parent or neighboring ions and thus defines the population of the state to which electron collisions occur in the presence of the laser field $\mathbf{E}(t)$. The time profiles of harmonics are obtained via a Gabor transform [34,35] of the time-dependent dipole acceleration which includes phase effects:

$$\ddot{d}_G(\omega,t) = \int_{-\infty}^{\infty} e^{-i\omega t'} e^{-\frac{(t'-t)^2}{2\sigma_0^2}} \langle\ddot{\varsigma}(t')\rangle dt'. \tag{11}$$

$\sigma_0 = 0.075$ fs is the width of the Gaussian time window in the Gabor transform, covering $N \approx 10$ harmonics in the analysis

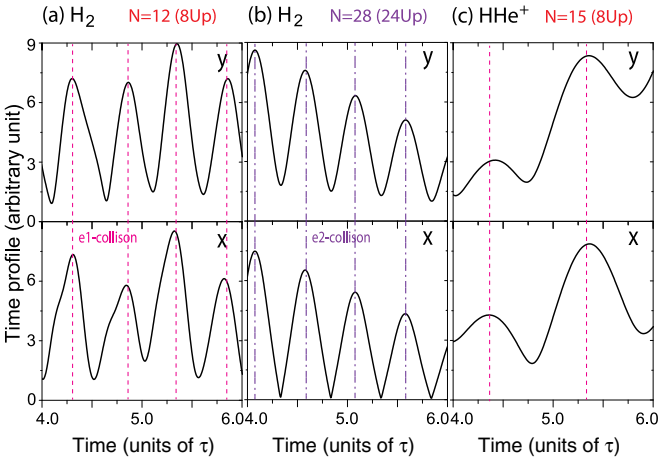

FIG. 3. (Color online) x and y components of time profiles of corresponding harmonics obtained from the Gabor transform for (a) H_2 at orders $(I_p + 8U_p)/\omega_0 = 12$ and (b) $(I_p + 24U_p)/\omega_0 = 28$ and (c) HHe^+ $(I_p + 8U_p)/\omega_0 = 15$ (cf. Fig. 1). Dashed (red) and dash-dotted (purple) lines indicate the collision time of the first ($e1$) and the second ($e2$) electrons.

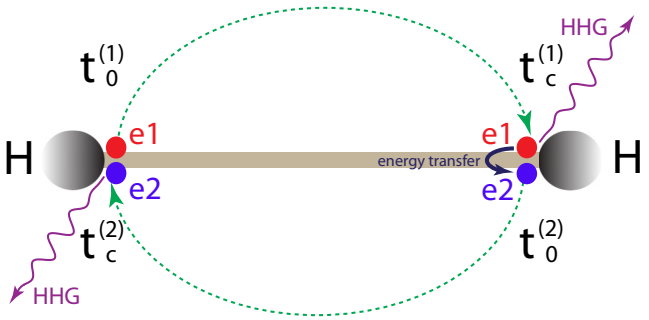

FIG. 4. (Color online) Illustration of laser induced electron collision in sequential double ionization of extended H_2. $e1$ (red ball) and $e2$ (blue ball) are the two delocalized electrons on protons (gray ball), and green dotted lines denote their trajectories. $t_0^{(1)}$ and $t_0^{(2)}$ are the ionization times and $t_c^{(1)}$ and $t_c^{(2)}$ are the collision times. A collision between $e1$ and $e2$ occurs on the right proton at times $t_c^{(1)} = t_0^{(2)}$. The thick arrow indicates the energy transfer due to collisions. Purple arrows represent HHG with energies (right) $I_p + 8U_p$ by collision of $e1$ with the ion at $t_c^{(1)}$ and (left) $I_p + 24U_p$ by collision of $e2$ at $t_c^{(2)}$.

for $\omega_0 = 0.114$ a.u. ($\lambda = 400$ nm). From Eqs. (7)–(10) we note that to obtain maximum kinetic energies $8U_p$ the phases should satisfy the relation $\omega_0 t_0 = -0.32\pi$ and $\omega_0 t_c - \omega_0 t_0 = \pi$ for $n' = 0$, i.e., the ionization time $t_0 = -0.16\tau$ or 0.34τ and the corresponding collision time $t_c = 0.34\tau$ and 0.84τ, where the electron displacements $x(t_c) = R = 22$ a.u. and $y(t_c) = 0$ in Eq. (10). The predictions are in good agreement with results of time profile analysis of harmonics at orders $(I_p + 8U_p)/\omega_0$ in Figs. 3(a) and 3(c), and evolutions of electron wave packets in Fig. 2. For HHe^+ initial localized electron density distributions on He give rise to *single* collision trajectory at H in each cycle.

In the symmetric H_2 with two delocalized (entangled by symmetry) electrons on the proton centers their ionization and collision times are different. From Eqs. (7)–(10) we obtain that the collision times $t_c^{(1)}$ of the ionized electron ($e1$) can also be the ionization time $t_0^{(2)}$ of the second electron ($e2$). Fox example, to collide with their neighboring ions, the *ionization* times for $e1$ and $e2$ are, respectively, $t_0^{(1)} = -0.16\tau$ and $t_0^{(2)} = 0.34\tau$, and the corresponding *collision* times are $t_c^{(1)} = 0.34\tau$ and $t_c^{(2)} = 0.84\tau$. At the time $t_c^{(1)} = t_0^{(2)}$, $e1$ can collide with $e2$ on the neighboring (right) proton center, as illustrated in Fig. 4. Following an energy transfer between electrons $e1$ and $e2$, $e2$ is ionized with a nonzero initial velocity v_{0c}. We therefore regard this process as a laser induced *sequential* double ionization. The corresponding laser induced velocities of $e2$ are

$$\dot{x}(t') = -\frac{E_0}{\omega_0}(\sin\omega_0 t' - \sin\omega_0 t_c) + v_{x0c},$$
$$\dot{y}(t') = -\frac{E_0}{\omega_0}(\cos\omega_0 t_c - \cos\omega_0 t') + v_{y0c}, \tag{12}$$

where t' is the time after electron collision and $t' > t_c$ and the "initial" velocity of $e2$ is $v_{0c} = \sqrt{v_{x0c}^2 + v_{y0c}^2}$. After recollision of $e2$ with its second neighboring ion, the resulting kinetic energy at time t_{cc} ($t_c^{(2)}$) based on Eq. (12) gives

$$K_e(t_{cc}) = \tfrac{1}{2}[\dot{x}^2(t_{cc}) + \dot{y}^2(t_{cc})] = \tfrac{1}{2}[v_{0c} + v'(t_{cc})]^2, \tag{13}$$

where $v'(t_{cc})$ is the laser induced velocity of $e2$. The corresponding displacements $x(t_{cc}) = y(t_{cc}) = 0$. For an elastic collision between $e1$ and $e2$, the initial velocity of the second electron is $|v_{0c}| = |v(t_c)|$ corresponding to energy $8U_p$. Assuming $v'(t_{cc}) = v(t_c)$, one finds final maximum energy $32U_p$.

For HHe^+, the electron distribution is strongly asymmetric due to initial localization on He, and the electron-electron collision on H is negligible. As a result no energy transfer occurs and an extended harmonic order is not generated, Fig. 1(b). For H_2 in Eq. (13) the energy transfer by electron collisions gives rise to HHG up to orders $(I_p + 24U_p)/\omega_0$. From Fig. 3(b) we see that the collision of $e2$ with neighboring ions occurs at $\omega_0 t_{cc} = 0.5n'\pi + 1.2\pi$, as illustrated in Fig. 2(a). The maximum order at $24U_p$ is slightly less than the predictions from Eq. (13). This suggests that inelastic scattering of electrons and molecular Coulomb potentials reduce the efficiency of energy transfer.

Finally we compare with linear polarization. The results of HHG spectra for x aligned H_2 by linearly polarized $\lambda = 400$ nm and $I_0 = 2 \times 10^{14}$ W/cm^2 are displayed in Fig. 5. We choose from the laser induced electron collision model in Eqs. (7)–(10), the molecular internuclear distances $R = 18$ and 9 a.u. By collision with neighboring ions with phase difference $\omega_0 t - \omega_0 t_0 = \pi$ and $\pi/2$, the maximum kinetic energies $8U_p$ and $6U_p$ can be obtained, exceeding the same parent ion recollision energy $3.17U_p$ giving rise to cutoff at $N_m = (I_p + 8U_p)/\omega_0 = 13$ and $(I_p + 6U_p)/\omega_0 = 11$. Large orders 21 and 15 are nevertheless also obtained weakly which correspond to the maximum kinetic energies $16U_p$ and $12U_p$, twice the single electron model. These extended orders therefore indicate the possibility of electron-electron collision in linear polarization HHG processes also but with much lower intensity (by two orders of magnitude). Similar processes

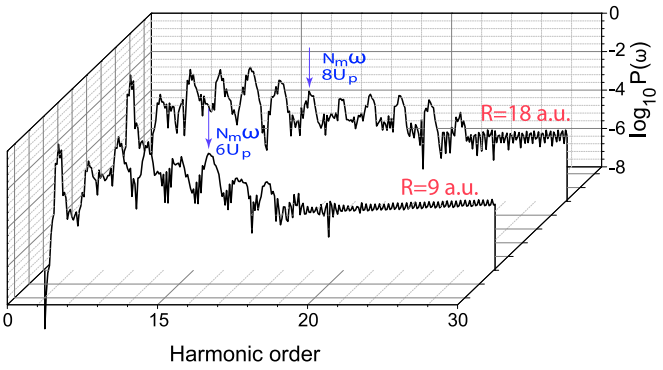

FIG. 5. (Color online) The x components of HHG spectra in x aligned H_2 at internuclear distance $R = 9$ and 18 a.u. with linearly polarized laser pulses at $I_0 = 2 \times 10^{14}$ W/cm^2 ($E_0 = 0.0755$ a.u.) and $\lambda = 400$ nm ($\omega = \omega_0 = 0.114$ a.u., $\tau = 1.33$ fs). The corresponding cutoff orders are, respectively, $N_m = (I_p + 6U_p)/\omega_0 \approx 11$ and $(I_p + 8U_p)/\omega_0 \approx 13$.

occur for single electron ionization with double collision of electrons [16,20].

IV. CONCLUSIONS

HHG spectra are investigated theoretically by circularly polarized laser pulses from numerical solutions of TDSEs for stretched (large internuclear distance) molecules. We derive a classical laser induced two electron collision model. Results show that for the entangled two electron H_2 harmonic spectra are obtained with energies $I_p + 24U_p$, which are attributed to energy exchange of electrons by collisions with each other in sequential double ionization. A time frequency analysis is used to clock collisions of electrons with ions to produce high-order harmonics, indicating the importance of electron entanglement in extending HHG plateaus. Harmonics for localized electron nonsymmetric HHe^+ molecular ions are also presented and compared, confirming the absence of electron-electron collision in this nonsymmetric case.

ACKNOWLEDGMENTS

The authors thank RQCHP and Compute Canada for access to massively parallel computer clusters and Natural Sciences and Engineering Research Council, FQRNT for financial support in their ultrafast science programs.

[1] P. B. Corkum and F. Krausz, Nat. Phys. **3**, 381 (2007).
[2] F. Krausz and M. Ivanov, Rev. Mod. Phys. **81**, 163 (2009).
[3] Z. Chang and P. Corkum, J. Opt. Soc. Am. B **27**, B9 (2010).
[4] K. Zhao, Q. Zhang, M. Chini, Y. Wu, X. Wang, and Z. Chang, Opt. Lett. **37**, 3891 (2012).
[5] P. B. Corkum, Phys. Rev. Lett. **71**, 1994 (1993); P. B. Corkum, N. H. Burnett, and F. Brunel, *ibid.* **62**, 1259 (1989).
[6] M. Lewenstein, P. Balcou, M. Y. Ivanov, A. L'Huillier, and P. B. Corkum, Phys. Rev. A **49**, 2117 (1994).
[7] G. L. Kamta and A. D. Bandrauk, Phys. Rev. A **71**, 053407 (2005).
[8] A. D. Bandrauk, S. Chelkowski, and S. Goudreau, J. Mod. Opt. **52**, 411 (2005).
[9] W. Becker, F. Grasbon, R. Kopold, D. B. Milošević, G. G. Paulus, and H. Walther, Adv. At. Mol. Opt. Phys. **48**, 35 (2002).
[10] D. B. Milošević and W. Becker, Phys. Rev. A **62**, 011403(R) (2000); D. B. Milošević, Opt. Lett. **40**, 2381 (2015).
[11] T. Zuo and A. D. Bandrauk, J. Nonlinear Opt. Phys. Mater. **04**, 533 (1995); A. D. Bandrauk and H. Z. Lu, Phys. Rev. A **68**, 043408 (2003).
[12] K. J. Yuan and A. D. Bandrauk, J. Phys. B **45**, 074001 (2012); Phys. Rev. Lett. **110**, 023003 (2013).
[13] A. D. Bandrauk, S. Chelkowski, H. Yu, and E. Constant, Phys. Rev. A **56**, R2537 (1997).
[14] P. Moreno, L. Plaja, and L. Roso, Phys. Rev. A **55**, R1593 (1997).
[15] A. D. Bandrauk, S. Barmaki, and G. L. Kamta, Phys. Rev. Lett. **98**, 013001 (2007).
[16] M. Lein and J. M. Rost, Phys. Rev. Lett. **91**, 243901 (2003).
[17] T. Pfeifer, D. Walter, G. Gerber, M. Yu. Emelin, M. Yu. Ryabikin, M. D. Chernobrovtseva, and A. M. Sergeev, Phys. Rev. A **70**, 013805 (2004).
[18] Q. Zhang, P. Lu, W. Hong, Q. Liao, P. Lan, and X. Wang, Phys. Rev. A **79**, 053406 (2009).
[19] M. Forre, E. Mével, and E. Constant, Phys. Rev. A **83**, 021402(R) (2011).
[20] K. J. Yuan and A. D. Bandrauk, Phys. Rev. A **84**, 023410 (2011).
[21] M. V. Frolov, N. L. Manakov, T. S. Sarantseva, M. Y. Emelin, M. Y. Ryabikin, and A. F. Starace, Phys. Rev. Lett. **102**, 243901 (2009).
[22] X. Wang and J. H. Eberly, Phys. Rev. Lett. **103**, 103007 (2009); X. Wang, J. Tian, and J. H. Eberly, *ibid.* **110**, 073001 (2013).
[23] F. Mauger, C. Chandre, and T. Uzer, Phys. Rev. Lett. **104**, 043005 (2010); **105**, 083002 (2010).
[24] A. N. Pfeiffer, C. Cirelli, M. Smolarski, R. Dörner, and U. Keller, Nat. Phys. **7**, 428 (2011); Y. Zhou, C. Huang, Q. Liao, and P. Lu, Phys. Rev. Lett. **109**, 053004 (2012).
[25] J. M. Ngoko Djiokap, N. L. Manakov, A. V. Meremianin, S. X. Hu, L. B. Madsen, and A. F. Starace, Phys. Rev. Lett. **113**, 223002 (2014).
[26] A. D. Bandrauk and H. Shen, J. Chem. Phys. **99**, 1185 (1993); A. D. Bandrauk and H. Z. Lu, J. Theor. Comput. Chem. **12**, 1340001 (2013).
[27] K.-J. Yuan, H. Z. Lu, and A. D. Bandrauk, Phys. Rev. A **83**, 043418 (2011).
[28] A. D. Bandrauk, S. Chelkowski, D. J. Diestler, J. Manz, and K. J. Yuan, Phys. Rev. A **79**, 023403 (2009).
[29] T. Ergler, A. Rudenko, B. Feuerstein, K. Zrost, C. D. Schröter, R. Moshammer, and J. Ullrich, Phys. Rev. Lett. **95**, 093001 (2005).
[30] E. Dehghanian, A. D. Bandrauk, and G. L. Kamta, J. Chem. Phys. **139**, 084315 (2013).
[31] K. Sodoga, J. Loreau, D. Lauvergnat, Y. Justum, N. Vaeck, and M. Desouter-Lecomte, Phys. Rev. A **80**, 033417 (2009).
[32] S. D. Khan, Y. Cheng, M. Möller, K. Zhao, B. Zhao, M. Chini, G. G. Paulus, and Z. Chang, Appl. Phys. Lett. **99**, 161106 (2011).
[33] J. H. Bauer, F. Mota-Furtado, P. F. O'Mahony, B. Piraux, and K. Warda, Phys. Rev. A **90**, 063402 (2014).
[34] P. Antoine, B. Piraux, and A. Maquet, Phys. Rev. A **51**, R1750 (1995).
[35] C. Chandre, S. Wiggins, and T. Uzer, Physica D **181**, 171 (2003).